Invariant Manifold and Bounds of Relative Motion Between Heliocentric Displaced Orbits

Wei Wang[1] and Jianping Yuan[2]

Northwestern Polytechnical University, 710072 Xi'an, People's Republic of China

National Key Laboratory of Aerospace of Flight Dynamics, 710072 Xi'an, People's Republic of China

Giovanni Mengali[3] and Alessandro A. Quarta[4]

University of Pisa, 56122 Pisa, Italy

Abstract In this paper, we establish a methodology for modeling relative motion between heliocentric displaced orbits by utilizing the Cartesian state variables in combination with a set of displaced orbital elements. Similar to classical Keplerian orbital elements, the newly defined set of displaced orbital elements has a clear physical meaning and provides an alternative approach to obtain a closed-form solution to the relative motion problem between displaced orbits, without linearizing or solving nonlinear equations. The invariant manifold of relative motion between two arbitrary displaced orbits is determined by coordinate transformations, obtaining a straightforward interpretation of the bounds, namely maximum and minimum relative distance of three directional components. The extreme values of these bounds are then calculated from an analytical viewpoint, both for quasi-periodic orbits in the incommensurable case and periodic orbits in the 1:1 commensurable case. Moreover, in some degenerate cases, the extreme values of relative distance bounds can also be solved analytically. For each case, simulation examples are discussed to validate the correctness of the proposed method.

1 Introduction

In recent years, non-Keplerian displaced orbits have attracted a considerable attention because of their unique advantages in astronomical missions [1-3], for example, in situ observation for Saturn's rings, solar wind monitoring, and real-time stereo-graphic investigations of a planetary surface [4-6]. Displaced orbits can be generated by suitable orienting the thrust direction induced by the sun in such a way to balance the centrifugal and gravitational components of the acceleration [1]. Spacecraft flying along displaced orbits can be promoted by new kinds of low thrust propulsion systems such as solar sails [2] and electric sails [3]. As a matter of fact, these orbits are very difficult to reach with conventional (either chemical or electric) propulsion systems. However, using solar sails as an example, some missions require an extremely large reflector area that cannot be carried out from an engineering standpoint [9], leaving it impractical to compromise between technical requirement and industrial manufacture in a near future. To that end, it is necessary to introduce the concept of formation flying, distributing multiple sails in a relatively proximate region and enabling them to construct a larger virtual sensor so as to achieve greater resolution than a single one. Nevertheless, up to now, studies of relative motion between displaced orbits obtained using photonic solar radiation pressure are scarce in the literature. Further, the linearized dynamic model was adopted among several existing ones [7-9], which were inherently limited to small-distance and short-term missions. Therefore, it is useful to gain a nonlinear insight into the relative motion problem, especially for the large baseline formation flying. Moreover, there have been few published

[1] Ph. D. Candidate, School of Astronautics; 418362467@qq.com.
[2] Professor, School of Astronautics; jyuan@nwpu.edu.cn.
[3] Professor, Dipartimento di Ingegneria Civile e Industriale; g.mengali@ing.unipi.it.
[4] Associate Professor, Dipartimento di Ingegneria Civile e Industriale; a.quarta@ing.unipi.it.

works to explore the relative motion bounds and topology in the general case of two sails flying along displaced orbits, which are of great importance in space mission's design and analysis, and therefore, they deserve a detailed study.

Recognizing these open issues, we first manage to model solar sail relative motion between displaced orbits with Cartesian relative state variables in conjunction with a newly established set of displaced orbital elements. Analogous to Keplerian orbital elements, the new set of parameters defines the orientation of a displaced orbit with respect to an inertial reference frame, as well as its real-time motion in rotating frame. Besides, utilizing coordinate transformations that incorporate displaced orbital elements, a closed-form solution expressed in a rotating frame can be derived without linearizing or solving the corresponding nonlinear equations. For the relative motion between circular displaced orbits, the solution is time-explicit, which is useful to analyze the nature of relative motion.

We also determine the relative motion invariant manifold, which is constituted by the parameterized general solution, and all possible orbits move along the manifold as they evolve. The invariant manifold presents a well-defined region in the configuration space with certain clear bounds, and the orbits moving on the manifold manifest periodicity for the commensurable case and quasi-periodicity (ergodicity) for the incommensurable case. The referred bounds in this paper are indeed extreme distances of radial, along-track and cross-track motion, as well as relative distance between two spacecraft flying along displaced orbits. The directional bounds are determined from an analytical viewpoint, both for the incommensurable case and 1:1 commensurable case, and the relative distance bounds can be calculated analytically in some degenerate cases. Analytical calculation of these bounds is essential for onboard on-off control when the relative distance arrives at the pre-set boundary, while the prediction of relative motion bounds by pure numerical integration is time consuming and may lead to time delays in inner communication. Moreover, to maintain a long-term cluster flight or loosed formation around displaced orbits, the designers may select proper elements to guarantee the limited-size mission requirement.

2 Relative Motion Between Heliocentric Displaced Orbits

To formulate the problem conveniently, first introduce the following related coordinate systems, seen in Fig. 1:

1) $\mathcal{I}$ is a heliocentric inertial frame, centered at the Sun, denoted by O. The fundamental plane is the ecliptic plane, the unit vector $\hat{\boldsymbol{X}}$ is directed from the Sun's center along the vernal equinox, $\hat{\boldsymbol{Z}}$ is normal to the fundamental plane, positive in the direction of the celestial north, and $\hat{\boldsymbol{Y}} = \hat{\boldsymbol{Z}} \times \hat{\boldsymbol{X}}$.

2) $\mathcal{R}$ is a rotating frame, centered at the spacecraft, denoted by S. The fundamental plane is the orbital plane with its origin o, the unit vector $\hat{\boldsymbol{x}}$ is in the radially outward direction, $\hat{\boldsymbol{z}}$ is normal to the orbital plane, positive in the direction of the angular momentum vector, and $\hat{\boldsymbol{y}} = \hat{\boldsymbol{z}} \times \hat{\boldsymbol{x}}$.

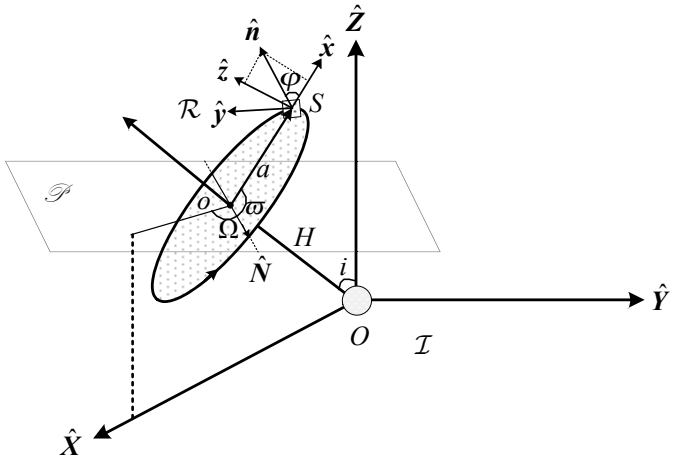

Fig. 1 Coordinate systems and related angles

In this context, assume that the spacecraft flying along displaced orbit is propelled by a solar sail. A heliocentric circular displaced orbit can be obtained by directing the thrust vector so as to have a component normal to the displaced orbital plane. The sail orientation is defined by the unit vector $\hat{\boldsymbol{n}}$ normal to the reflecting surface, fixed in the rotating frame $\mathcal{R}$. The performance is characterized by the dimensionless lightness number β, defined as the ratio of the propulsion acceleration to the solar gravitational acceleration, that is $\beta = 1.529/\sigma\ \left(\mathrm{g}\cdot\mathrm{m}^{-2}\right)$, where σ is the sail mass per unit area. For a given orbital angular velocity ω, a displaced orbital radius a, and a displacement H from the Sun, the following relationships should hold so as to keep equilibrium in $\mathcal{R}$ [4]

$$tan\varphi = \frac{H}{a}\frac{1}{1-\left(\omega/\omega_*\right)^2} \tag{1}$$

$$\beta = \left[1+\left(H/a\right)^2\right]^{\frac{1}{2}}\frac{\left\{\left(H/a\right)^2+\left[1-\left(\omega/\omega_*\right)^2\right]^2\right\}^{\frac{3}{2}}}{\left[\left(H/a\right)^2+1-\left(\omega/\omega_*\right)^2\right]^2} \tag{2}$$

where $\omega_* \triangleq \sqrt{\mu/r^3}$, $r=\sqrt{a^2+H^2}$ is the Sun-sail distance, and φ is the angle related to the attitude of the sail.

2.1 Set of Displaced Orbital Elements

In the classical two-body problem, the orbital motion in three-dimensional space can be described either by the state vector $\boldsymbol{S}_{Keplerian}=\left[\boldsymbol{r},\boldsymbol{v}\right]\in\mathbb{R}^3\times\mathbb{R}^3$, or a set of orbital elements $\boldsymbol{\varpi}_{Keplerian}=\left[a,e,i,\Omega,\omega,f\right]\in\mathbb{R}^2\times\mathbb{S}^4$, where $\mathbb{R}$ and $\mathbb{S}$ denote the real number space and spherical space respectively. The state vector is convenient for onboard measurement, while the orbital elements provide a straightforward understanding of the orbital orientation with respect to the inertial frame, as well as real-time on-orbit location. However, for some Keplerian cases, the Eulerian angles Ω, ω may become undefined [11-13]. Since the displaced orbit is assumed circular in this paper, we shall define a new set of nonsingular displaced orbital elements $\boldsymbol{\varpi}_{Displaced}$ to characterize the motion.

First, locate the intersection of the orbital plane with plane $\mathscr{P}$, which is parallel to the ecliptic plane and passes through the center o of the displaced orbit. The intersection is the line of nodes, and the point on that line where the orbit passes above the plane $\mathscr{P}$ from the below is called the ascending node. The unit vector directed from the center o to the ascending node is denoted by $\hat{\boldsymbol{N}}$, see Fig.1. The circular displaced orbital elements are defined as follows:

a : displaced orbital radius;

i : inclination, the angle between the orbital plane and the ecliptic plane, measured according to the right-handed rule, counterclockwise from the positive $\hat{\boldsymbol{Z}}$ axis to the normal to the orbital plane;

Ω : right ascension of the ascending node, the angle measured from the positive $\hat{\boldsymbol{X}}$ axis to the line of nodes;

ϖ : mean argument of latitude, measured from $\hat{\boldsymbol{N}}$ to the position vector $\boldsymbol{r}$.

From Eq. (1), note that for a given pair of a and H, the angular velocity ω depends on the angle φ. In this paper, φ is assumed to be fixed by means of a passive control [14]. The transformation procedure between the state vector $\boldsymbol{S}_{Displaced}=\left[\boldsymbol{r},\boldsymbol{v}\right]_{\mathcal{I}}$ in frame $\mathcal{I}$ and the displaced orbital elements $\boldsymbol{\varpi}_{Displaced}$ is as follows.

1) $\boldsymbol{\varpi}_{Displaced}\mapsto\boldsymbol{S}_{Displaced}$.

A. For a given pair β and φ, calculate ω and H from Eqs. (1) and (2).

B. Calculate the state vector in the frame $\mathcal{R}$:

$$[\boldsymbol{r}]_{\mathcal{R}} = [a, \quad 0, \quad H]^T, \quad [\boldsymbol{v}]_{\mathcal{R}} = [0, \quad \omega a, \quad 0]^T \tag{3}$$

C. Calculate $[\boldsymbol{r}]_{\mathcal{I}}$ and $[\boldsymbol{v}]_{\mathcal{I}}$ using the coordinate transformation $\mathcal{R} \to \mathcal{I}$. The directional cosines matrix is given by:

$$T_{\mathcal{R}\to\mathcal{I}}(\Omega, i, \varpi) = T_z(-\Omega) T_x(-i) T_z(-\varpi) \tag{4}$$

where

$$T_x(\cdot) = \begin{bmatrix} 1 & 0 & 0 \\ 0 & \cos(\cdot) & \sin(\cdot) \\ 0 & -\sin(\cdot) & \cos(\cdot) \end{bmatrix}, \quad T_z(\cdot) = \begin{bmatrix} \cos(\cdot) & \sin(\cdot) & 0 \\ -\sin(\cdot) & \cos(\cdot) & 0 \\ 0 & 0 & 1 \end{bmatrix} \tag{5}$$

$$T_{\mathcal{R}\to\mathcal{I}} \triangleq \begin{bmatrix} \cos\varpi\cos\Omega - \sin\varpi\cos i\sin\Omega & -\sin\varpi\cos\Omega - \cos\varpi\cos i\sin\Omega & \sin i\sin\Omega \\ \cos\varpi\sin\Omega + \sin\varpi\cos i\cos\Omega & -\sin\varpi\sin\Omega + \cos\varpi\cos i\cos\Omega & -\sin i\cos\Omega \\ \sin\varpi\sin i & \cos\varpi\sin i & \cos i \end{bmatrix} \tag{6}$$

The state vector in the frame $\mathcal{I}$ is therefore expressed as

$$[\boldsymbol{r}]_{\mathcal{I}} = T_{\mathcal{R}\to\mathcal{I}} \cdot [\boldsymbol{r}]_{\mathcal{R}}, \quad [\boldsymbol{v}]_{\mathcal{I}} = T_{\mathcal{R}\to\mathcal{I}} \cdot [\boldsymbol{v}]_{\mathcal{R}} \tag{7}$$

2) $\boldsymbol{S}_{Displaced} \mapsto \boldsymbol{\alpha}_{Displaced}$.

A. Calculate the modulus of the state vector:

$$\|\boldsymbol{r}\| = \sqrt{\boldsymbol{r}\cdot\boldsymbol{r}}, \quad \|\boldsymbol{v}\| = \sqrt{\boldsymbol{v}\cdot\boldsymbol{v}} \tag{8}$$

B. Calculate a and ω by combining Eqs. (1), (2) and (8), then determine $\boldsymbol{\omega}$ using the following equations:

$$\boldsymbol{\omega}\cdot\boldsymbol{v} = 0 \tag{9}$$

$$\boldsymbol{\omega}\cdot\boldsymbol{r} = \omega a \tag{10}$$

$$\|\boldsymbol{\omega}\| = \omega \tag{11}$$

C. Calculate i:

$$i = \arccos\left(\hat{\boldsymbol{\omega}}\cdot\hat{\boldsymbol{Z}}\right) \tag{12}$$

D. Calculate $\hat{\boldsymbol{N}}$:

$$\hat{\boldsymbol{N}} = \left(\hat{\boldsymbol{Z}}\times\hat{\boldsymbol{\omega}}\right) \Big/ \left\|\hat{\boldsymbol{Z}}\times\hat{\boldsymbol{\omega}}\right\| \tag{13}$$

E. Calculate Ω from Eq. (13):

$$\Omega = \arccos\left(\hat{\boldsymbol{N}}\cdot\hat{\boldsymbol{X}}\right) \tag{14}$$

F. Calculate ϖ utilizing Eq. (13):

$$\varpi = \arccos\left(\hat{\boldsymbol{r}}\cdot\hat{\boldsymbol{N}}\right) \tag{15}$$

In essence, the introduction of the new set of displaced orbital elements is useful for modeling relative motion between displaced orbits and obtaining a closed-form solution to the relative motion problem, as will be shown in the next section.

2.2 Nonlinear Equations Establishment

In this section, we shall study the relative motion modeling between two heliocentric displaced orbits. The sail that tracks a given reference orbit, is referred to as the chief (subscript *C*), and the other is called the deputy (subscript *D*). The fundamental equations of the two sails under Newtonian central-body gravitation and solar radiation pressure acceleration can be written as

$$\frac{d^2\boldsymbol{r}_C}{dt^2} = -\frac{\mu}{r_C^3}\boldsymbol{r}_C + \beta_C\left(\hat{\boldsymbol{n}}_C\cdot\boldsymbol{r}_C\right)^2\frac{\mu}{r_C^4}\hat{\boldsymbol{n}}_C \tag{16}$$

$$\frac{d^2\boldsymbol{r}_D}{dt^2} = -\frac{\mu}{r_D^3}\boldsymbol{r}_D + \beta_D\left(\hat{\boldsymbol{n}}_D\cdot\boldsymbol{r}_D\right)^2\frac{\mu}{r_D^4}\hat{\boldsymbol{n}}_D \tag{17}$$

Let $\boldsymbol{\rho} = \boldsymbol{r}_D - \boldsymbol{r}_C$ denote the relative position and $\alpha \in [0,\pi/2]$ be the thrust pitch angle between $\hat{\boldsymbol{n}}$ and $\boldsymbol{r}$, then the relative acceleration expressed in the frame $\mathcal{I}$ is obtained by subtracting Eq. (16) from Eq. (17)

$$\frac{d^2\boldsymbol{\rho}}{dt^2} = -\frac{\mu}{r_D^3}\boldsymbol{r}_D + \frac{\mu}{r_C^3}\boldsymbol{r}_C + \beta_D\cos^2\alpha_D\frac{\mu}{r_D^2}\hat{\boldsymbol{n}}_D - \beta_C\cos^2\alpha_C\frac{\mu}{r_C^2}\hat{\boldsymbol{n}}_C \tag{18}$$

We can also utilize the following relationship

$$\frac{d^2\boldsymbol{\rho}}{dt^2} = \ddot{\boldsymbol{\rho}} + 2\boldsymbol{\omega}_C\times\dot{\boldsymbol{\rho}} + \boldsymbol{\omega}_C\times\left(\boldsymbol{\omega}_C\times\boldsymbol{\rho}\right) + \dot{\boldsymbol{\omega}}_C\times\boldsymbol{\rho} \tag{19}$$

where the dot symbol represents a time derivative taken in the rotating frame.

As $\boldsymbol{\omega}_C$ is normal to the orbital plane, and in our case, $\dot{\boldsymbol{\omega}}_C = \boldsymbol{0}$, we can write

$$\left[\boldsymbol{\omega}_C\right]_{\mathcal{R}_C} = \left[0,\quad 0,\quad \dot{\varpi}_C\right]^T = \left[0,\quad 0,\quad \omega_C\right]^T \tag{20}$$

The position vector of the chief is given by

$$\left[\boldsymbol{r}_C\right]_{\mathcal{R}_C} = \left[a_C,\quad 0,\quad H_C\right]^T \tag{21}$$

The relative position vector is written as

$$\left[\boldsymbol{\rho}\right]_{\mathcal{R}_C} = \left[x,\quad y,\quad z\right]^T \tag{22}$$

Because we assume that the angle φ is fixed in the frame $\mathcal{R}$, the unit vector $\hat{\boldsymbol{n}}_C$ is therefore

$$\left[\hat{\boldsymbol{n}}_C\right]_{\mathcal{R}_C} = \left[\cos\varphi_C,\quad 0,\quad \sin\varphi_C\right]^T \tag{23}$$

The unit vector $\hat{\boldsymbol{n}}_D$ in the frame $\mathcal{R}_C$ can be obtained through coordinate transformations:

$$\left[\hat{\boldsymbol{n}}_D\right]_{\mathcal{R}_C} = T_{\mathcal{I}\to\mathcal{R}_C}\left(\Omega_C,i_C,\varpi_C\right)\cdot T_{\mathcal{R}_D\to\mathcal{I}}\left(\Omega_D,i_D,\varpi_D\right)\cdot\left[\cos\varphi_D,\quad 0,\quad \sin\varphi_D\right]^T \tag{24}$$

Substituting Eqs. (19) - (24) into Eq. (18) yields a set of nonlinear differential equations expressed in the frame $\mathcal{R}_C$, written in terms of relative state in combination with displaced orbital elements:

$$\begin{cases} \ddot{x} - 2\omega_C\dot{y} - \omega_C^2 x = \dfrac{\mu a_C}{\left(a_C^2+H_C^2\right)^{\frac{3}{2}}} - \dfrac{\mu\left(a_C+x\right)}{\left[\left(a_C+x\right)^2+y^2+\left(H_C+z\right)^2\right]^{\frac{3}{2}}} + \dfrac{\mu\beta_D\cos^2\alpha_D\hat{n}_D(1)}{\left(a_C+x\right)^2+y^2+\left(H_C+z\right)^2} - \dfrac{\mu\beta_C\cos^2\alpha_C\cos\varphi_C}{a_C^2+H_C^2} \\ \ddot{y} + 2\omega_C\dot{x} - \omega_C^2 y = -\dfrac{\mu y}{\left[\left(a_C+x\right)^2+y^2+\left(H_C+z\right)^2\right]^{\frac{3}{2}}} + \dfrac{\mu\beta_D\cos^2\alpha_D\hat{n}_D(2)}{\left(a_C+x\right)^2+y^2+\left(H_C+z\right)^2} \\ \ddot{z} = \dfrac{\mu H_C}{\left(a_C^2+H_C^2\right)^{\frac{3}{2}}} - \dfrac{\mu\left(H_C+z\right)}{\left[\left(a_C+x\right)^2+y^2+\left(H_C+z\right)^2\right]^{\frac{3}{2}}} + \dfrac{\mu\beta_D\cos^2\alpha_D\hat{n}_D(3)}{\left(a_C+x\right)^2+y^2+\left(H_C+z\right)^2} - \dfrac{\mu\beta_C\cos^2\alpha_C\sin\varphi_C}{a_C^2+H_C^2} \end{cases} \tag{25}$$

where $\hat{n}_D(k)$ is the k-th entry of vector $[\hat{\boldsymbol{n}}_D]_{\mathcal{R}_C}$, and

$$[\hat{\boldsymbol{n}}_D]_{\mathcal{R}_C} = \begin{bmatrix} \cos\varphi_D \sum_{k=1}^{3} T_C(k,1)T_D(k,1) + \sin\varphi_D \sum_{k=1}^{3} T_C(k,1)T_D(k,3) \\ \cos\varphi_D \sum_{k=1}^{3} T_C(k,2)T_D(k,1) + \sin\varphi_D \sum_{k=1}^{3} T_C(k,2)T_D(k,3) \\ \cos\varphi_D \sum_{k=1}^{3} T_C(k,3)T_D(k,1) + \sin\varphi_D \sum_{k=1}^{3} T_C(k,3)T_D(k,3) \end{bmatrix} \tag{26}$$

where $T_C(i,j)$ and $T_D(i,j)$ are given in Eq. (6). Eq. (25) is the basic dynamic equation of relative motion between two heliocentric displaced orbits. In general, it is difficult to carry out the stability performance directly. One feasible approach is to study the stable region numerically for a given set of parameters.

3. General Solution and Invariant Manifold of Relative Motion via Displaced Orbital Elements

In this section, we shall derive a general solution to the relative motion problem using Eulerian transformations, instead of linearizing the problem, in order to avoid possible errors. To express the relative position in the chief's rotating frame $\mathcal{R}_C$, we may use the frame $\mathcal{I}$ as an intermediate bridge [15]. The first step is to transform the deputy's position vector from frame $\mathcal{R}_D$ to frame $\mathcal{I}$, and then operate a similar transformation from frame $\mathcal{I}$ to frame $\mathcal{R}_C$. The second step is to obtain the relative position by subtracting the two position vectors expressed in the frame $\mathcal{R}_C$. In transformations, the related Eulerian angles are Ω, i and ϖ respectively. The relative position vector $\boldsymbol{\rho}$ is therefore

$$[\boldsymbol{\rho}]_{\mathcal{R}_C} = T_{\mathcal{I}\to\mathcal{R}_C}(\Omega_C, i_C, \varpi_C) \cdot T_{\mathcal{R}_D\to\mathcal{I}}(\Omega_D, i_D, \varpi_D) \cdot [a_D, \quad 0, \quad H_D]^T - [a_C, \quad 0, \quad H_C]^T \tag{27}$$

The components of the relative position vector $\boldsymbol{\rho}$ is written as

$$[\boldsymbol{\rho}]_{\mathcal{R}_C} = \begin{bmatrix} a_D \sum_{k=1}^{3} T_C(k,1)T_D(k,1) + H_D \sum_{k=1}^{3} T_C(k,1)T_D(k,3) - a_C \\ a_D \sum_{k=1}^{3} T_C(k,2)T_D(k,1) + H_D \sum_{k=1}^{3} T_C(k,2)T_D(k,3) \\ a_D \sum_{k=1}^{3} T_C(k,3)T_D(k,1) + H_D \sum_{k=1}^{3} T_C(k,3)T_D(k,3) - H_C \end{bmatrix} \tag{28}$$

After some mathematical operations, Eq. (28) can be expressed in a compact form

$$[\boldsymbol{\rho}]_{\mathcal{R}_C} = a_D \begin{bmatrix} \xi_1 \cos\varpi_C \cos\varpi_D - \xi_2 \cos\varpi_C \sin\varpi_D + \xi_4 \sin\varpi_C \cos\varpi_D + \xi_3 \sin\varpi_C \sin\varpi_D - \xi_5 \cos\varpi_C + \xi_6 \sin\varpi_C - a_C/a_D \\ \xi_4 \cos\varpi_C \cos\varpi_D + \xi_3 \cos\varpi_C \sin\varpi_D - \xi_1 \sin\varpi_C \cos\varpi_D + \xi_2 \sin\varpi_C \sin\varpi_D + \xi_6 \cos\varpi_C + \xi_5 \sin\varpi_C \\ -\xi_7 \cos\varpi_D + \xi_8 \sin\varpi_D + \xi_9 - H_C/a_D \end{bmatrix} \tag{29}$$

where

$$\xi_1 \triangleq \cos(\Omega_C - \Omega_D) \tag{30}$$

$$\xi_2 \triangleq \cos i_D \sin(\Omega_D - \Omega_C) \tag{31}$$

$$\xi_3 \triangleq \left[\cos i_C \cos i_D \cos(\Omega_C - \Omega_D) + \sin i_C \sin i_D\right] \tag{32}$$

$$\xi_4 \triangleq \cos i_C \sin(\Omega_D - \Omega_C) \tag{33}$$

$$\xi_5 \triangleq H_D/a_D \sin i_D \sin(\Omega_C - \Omega_D) \tag{34}$$

$$\xi_6 \triangleq H_D/a_D\left[\sin i_C \cos i_D - \cos i_C \sin i_D \cos\left(\Omega_C - \Omega_D\right)\right] \tag{35}$$

$$\xi_7 \triangleq \sin i_C \sin\left(\Omega_D - \Omega_C\right) \tag{36}$$

$$\xi_8 \triangleq \cos i_C \sin i_D - \cos i_D \sin i_C \cos\left(\Omega_C - \Omega_D\right) \tag{37}$$

$$\xi_9 \triangleq H_D/a_D\left[\cos i_C \cos i_D + \sin i_C \sin i_D \cos\left(\Omega_C - \Omega_D\right)\right] \tag{38}$$

The closed-form solution in the three-dimensional configuration space constitutes the invariant manifold $\Re$, on which the relative motion will evolve all the time. The expression of $\boldsymbol{\rho}$ contains two angular coordinates, $\left(\varpi_C, \varpi_D\right) \in \mathbb{S}^1 \times \mathbb{S}^1$, and the invariant manifold $\Re$ is, most likely, a typical space with continuous surfaces of a cylinder, torus (toroid), sphere, or truncated cone [16], etc. Such a manifold has the appearance of a smooth surface and can be treated as a two-dimensional Euclidean space.

There are two qualitatively different cases, depending on whether the natural frequencies are commensurable or not. For the commensurable case, the ratio of the frequencies is rational, satisfying $\omega_C/\omega_D = p/q$, where $p,q \in \mathbb{N}$, and $\mathbb{N}$ denotes the set of natural numbers. All possible orbits in this case are closed curves on $\Re$. In practice, the 1:1 commensurability is more preferable in the engineering sense, because most of the formation flying missions require periodic relative motion on short time scales. For the incommensurable case where the ratio of the frequencies is irrational, the flow on $\Re$ is referred to as two-periodic quasi-periodic. This type of orbit unfolds along a helix on the surface of $\Re$, meandering over the whole region of $\Re$. However, every orbit winds around endlessly, never intersecting itself and yet never quite closing. For this case, the orbit is termed dense on $\Re$: in other words, each orbit comes arbitrarily close to any given point on $\Re$. This is not to say that the orbit passes through each point; it just comes arbitrarily close [17].

Consider a chief heliocentric displaced orbit, paralleled to the ecliptic plane. Note that Ω is undefined in this case, however, for the sake of simplicity in form and consistency in equations, we may treat Ω as a meaningless variable that can be set freely, without the need to introduce the mean longitude $l = \varpi + \Omega$ to eliminate the singularity [11], as is usually done. Notably this is not a restrictive assumption, as the final results are independent of Ω.

We use the normalized variables by setting $r_C = \mu = 1$. Let $\varphi_C = 45^\circ, \varphi_D = 60^\circ$, and the displaced orbital elements of the two sails are given by

$$\begin{aligned} \boldsymbol{\alpha}_C &= \left[\tilde{a}_C, i_C, \Omega_C, \varpi_C\right] = \left[0.8, 0^\circ, 0^\circ, \varpi_C\right] \\ \boldsymbol{\alpha}_D &= \left[\tilde{a}_D, i_D, \Omega_D, \varpi_D\right] = \left[2/\sqrt{7}, 5^\circ, 90^\circ, \varpi_D\right] \end{aligned} \tag{39}$$

where $\tilde{(\cdot)}$ denotes the normalized value. Using the parameters given above, we obtain $\tilde{\omega}_C = 0.5$, $\tilde{\omega}_D = \sqrt{0.5}$, $\tilde{H}_C = 0.6$, $\tilde{H}_D = \sqrt{3}/\sqrt{7}$, $\beta_C = 30\sqrt{2}/49$, $\beta_D = 8\sqrt{7}/25$.

Using Eq. (28), the closed-form solution of relative position becomes

$$\left[\boldsymbol{\rho}\right]_{\mathcal{R}_C} = \begin{bmatrix} x \\ y \\ z \end{bmatrix} = \begin{bmatrix} a_D\left(-\cos\varpi_C \sin\varpi_D \cos i_D + \sin\varpi_C \cos\varpi_D\right) + H_D \cos\varpi_C \sin i_D - a_C \\ a_D\left(\sin\varpi_C \sin\varpi_D \cos i_D + \cos\varpi_C \cos\varpi_D\right) - H_D \sin\varpi_C \sin i_D \\ a_D\left(\sin\varpi_D \sin i_D\right) + H_D \cos i_D - H_C \end{bmatrix} \tag{40}$$

Since the orbit is assumed circular, the mean arguments of latitude of the chief and deputy are written as

$$\begin{aligned} \varpi_C &= \omega_C \cdot t + \varpi_{C_0} \mod 2\pi \\ \varpi_D &= \omega_D \cdot t + \varpi_{D_0} \mod 2\pi \end{aligned} \tag{41}$$

where ϖ_{C_0} and ϖ_{D_0} are the initial mean arguments of latitude of the chief and deputy. It indicates that $\boldsymbol{\rho}$ can be expressed as an explicit function of time. This is of great importance and advantage in understanding the dynamic nature of relative motion between two displaced orbits. For example, it can be used to find the bounds of relative motion, as will be illustrated in Sec. 4. The components of the relative position vector in Eq. (40) can be further written as

$$\begin{aligned} x &= -\kappa_1 \cos\left(\omega_C t+\varpi_{C0}\right)\sin\left(\omega_D t+\varpi_{D0}\right)+\kappa_2 \sin\left(\omega_C t+\varpi_{C0}\right)\cos\left(\omega_D t+\varpi_{D0}\right)+\kappa_3 \cos\left(\omega_C t+\varpi_{C0}\right)+\kappa_4 \\ y &= \kappa_1 \sin\left(\omega_C t+\varpi_{C0}\right)\sin\left(\omega_D t+\varpi_{D0}\right)+\kappa_2 \cos\left(\omega_C t+\varpi_{C0}\right)\cos\left(\omega_D t+\varpi_{D0}\right)-\kappa_3 \sin\left(\omega_C t+\varpi_{C0}\right) \\ z &= \kappa_5 \sin\left(\omega_D t+\varpi_{D0}\right)+\kappa_6 \end{aligned} \tag{42}$$

where

$$\kappa_1 \triangleq a_D \cos i_D, \quad \kappa_2 \triangleq a_D, \quad \kappa_3 \triangleq H_D \sin i_D, \quad \kappa_4 \triangleq -a_C, \quad \kappa_5 \triangleq a_D \sin i_D, \quad \kappa_6 \triangleq H_D \cos i_D - H_C \tag{43}$$

Fig.2 shows the three-dimensional relative orbit (dotted line) lying on the invariant manifold $\Re$ (solid line). Since the ratio of the angular velocities $\tilde{\omega}_C/\tilde{\omega}_D = \sqrt{0.5}$ is an irrational number, the motion along $\Re$ is quasi-periodic. Fig.3 depicts the relative motion projected on *x*-*y*, *x*-*z*, and *y*-*z* planes respectively. It can be clearly seen that with the given conditions, the invariant manifold $\Re$ resembles a frustum of a cone with a curved rotation surface.

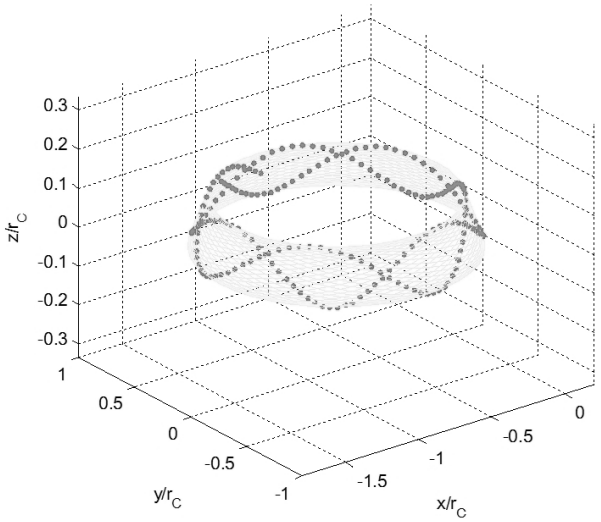

Fig. 2 Three-dimensional quasi-periodic relative motion and the invariant manifold it lies on

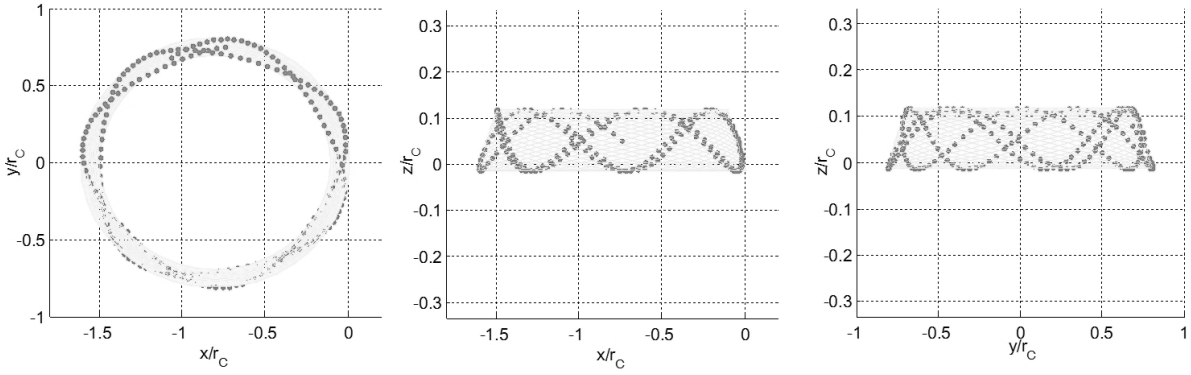

Fig. 3 Projections of quasi-periodic relative motion to *x*-*y*, *x*-*z*, and *y*-*z* planes

If the thrust pitch angle of the deputy is changed such as to guarantee the commensurability of the two angular velocities, then the relative motion turns to be periodic. For example, assuming $\varphi_D = \arctan 2/\sqrt{3}$, the normalized angular velocity of the deputy sail becomes $\tilde{\omega}_D = 0.5$, equal to that of the chief, therefore satisfying 1:1

commensurability (resonance). Fig.4 illustrates ten 1:1 commensurable periodic relative orbits that are evenly distributed on the invariant manifold $\Re$ with equal initial phase (mean argument of latitude) differences. Fig.5 illustrates the projections to *x*-*y*, *x*-*z*, and *y*-*z* planes.

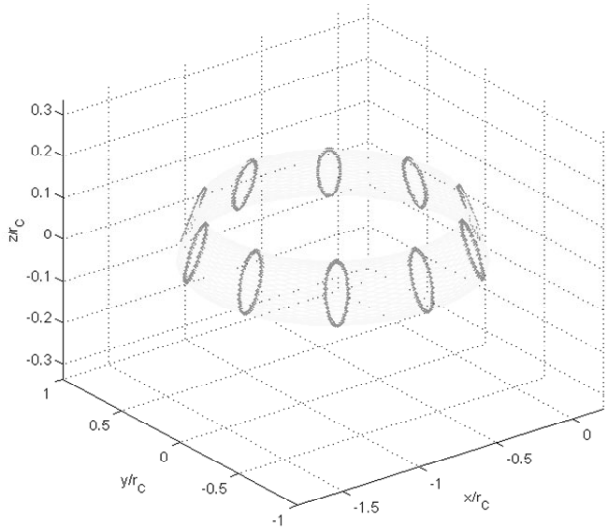

Fig. 4 Three-dimensional 1:1 commensurable periodic relative motion and the invariant manifold it lies on

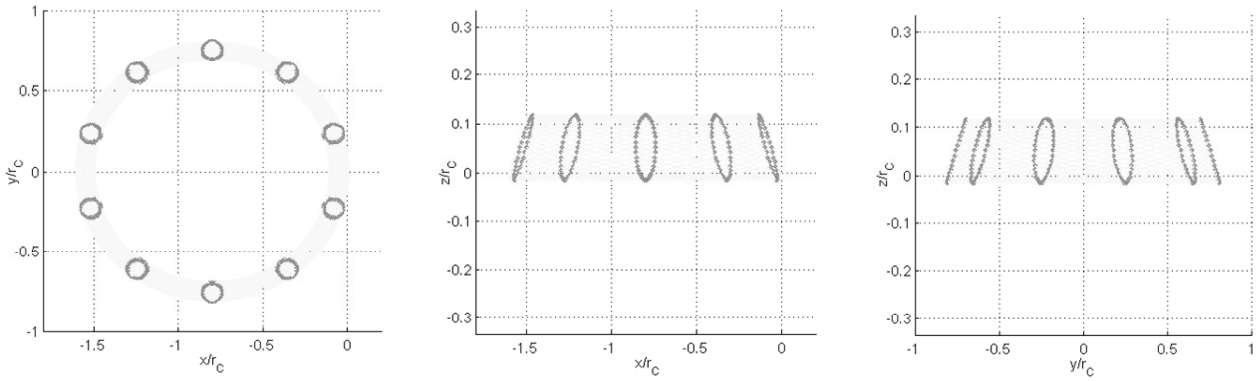

Fig. 5 Projections of 1:1 commensurable periodic relative motion to *x*-*y*, *x*-*z*, and *y*-*z* planes

Changing the ratio of the frequencies $\tilde{\omega}_C/\tilde{\omega}_D$, more types of commensurable periodic relative orbits are obtained. As is shown in Fig. 6, all closed curves starting on $\Re$ remain on $\Re$ for all time during the motion.

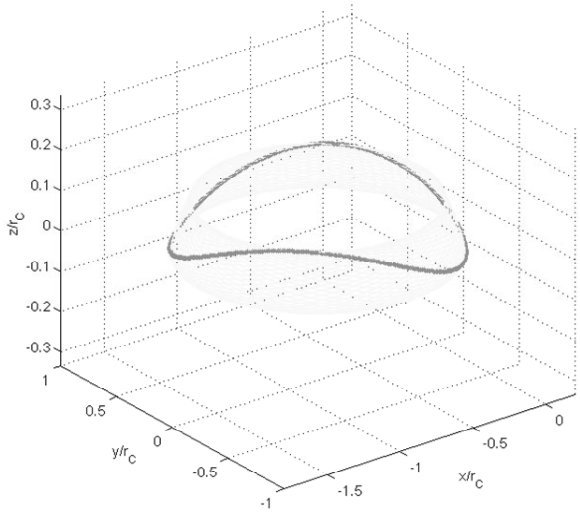

1:2 commensurability

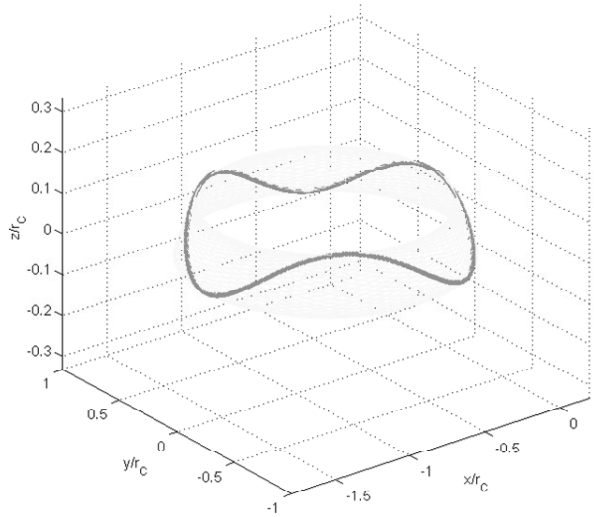

2:3 commensurability

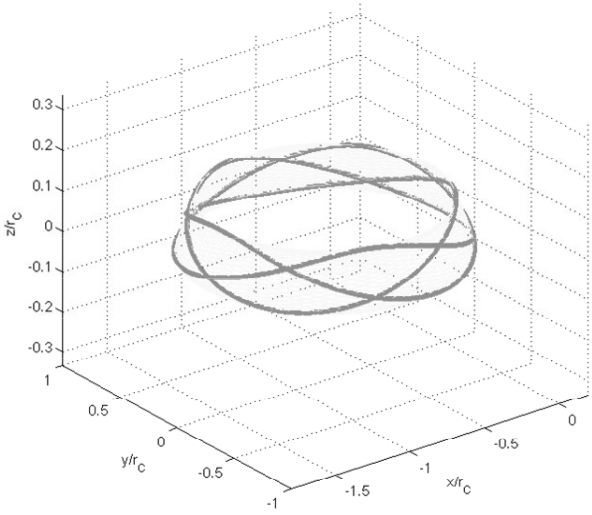

8:5 commensurability

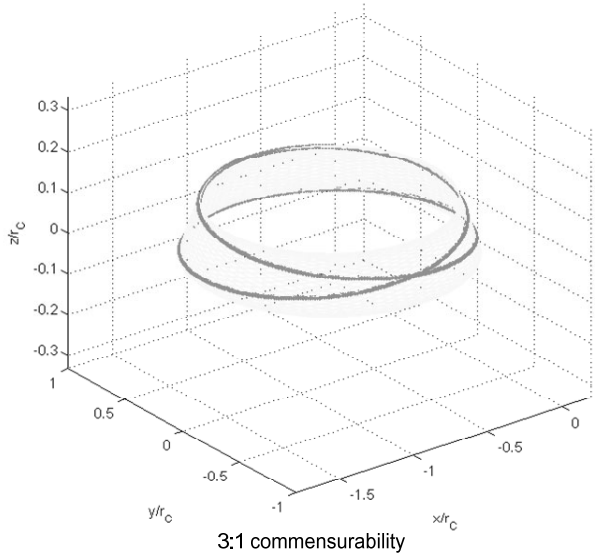

3:1 commensurability

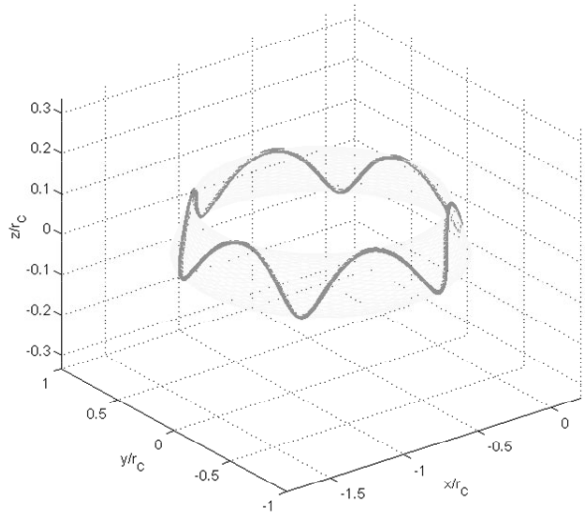

5:6 commensurability

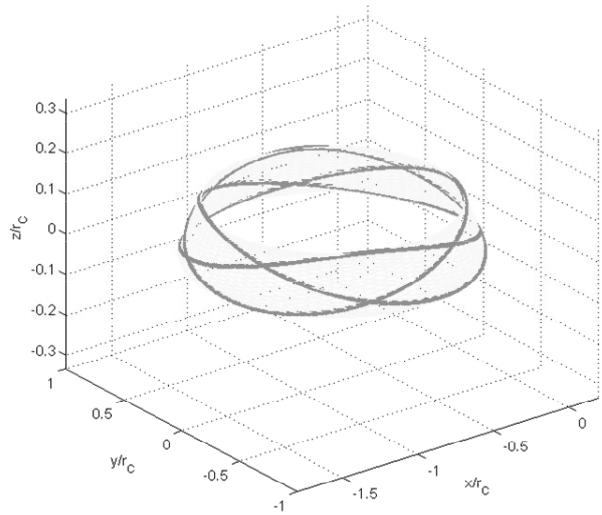

7:4 commensurability

Fig. 6 Other types of commensurable periodic relative orbits

4. Bounds of Relative Motion

As illustrated above, the relative motion between displaced orbits is always bounded, lying on invariant manifold $\Re$. In this section, the upper and lower bounds of each single directional motion for the incommensurable case and 1:1 commensurable case will be studied from an analytical point of view.

4.1 Bounds of Incommensurable Relative Orbit

Eq. (28) provides a parametric presentation of the relative motion invariant manifold between two displaced orbits. For the incommensurable case, the relative orbit is quasi-periodic and ergodic, so Eq. (28) can be used to seek for the extreme value points of the incommensurable relative orbit.

4.1.1 Radial bounds

To find the bounds of radial motion, the following relationship should hold

$$\frac{\partial x}{\partial \varpi_C} = a_D \sum_{k=1}^{3} \frac{\partial T_C(k,1)}{\partial \varpi_C} T_D(k,1) + H_D \sum_{k=1}^{3} \frac{\partial T_C(k,1)}{\partial \varpi_C} T_D(k,3) = 0 \tag{44}$$

$$\frac{\partial x}{\partial \varpi_D} = a_D \sum_{k=1}^{3} T_C(k,1) \frac{\partial T_D(k,1)}{\partial \varpi_D} + H_D \sum_{k=1}^{3} T_C(k,1) \frac{\partial T_D(k,3)}{\partial \varpi_D} = 0 \tag{45}$$

From Eq. (6), note that

$$\frac{\partial T_D(k,3)}{\partial \varpi_D} = 0, \quad k = 1,2,3 \tag{46}$$

Substituting Eq. (46) into Eqs. (44) and (45) results in

$$-\xi_1 \cdot \sin\varpi_C^* \cos\varpi_D^* + \xi_2 \cdot \sin\varpi_C^* \sin\varpi_D^* + \xi_3 \cdot \cos\varpi_C^* \sin\varpi_D^* + \xi_4 \cdot \cos\varpi_C^* \cos\varpi_D^* + \xi_5 \cdot \sin\varpi_C^* + \xi_6 \cdot \cos\varpi_C^* = 0 \tag{47}$$

$$\xi_3 \cdot \sin\varpi_C^* \cos\varpi_D^* - \xi_4 \cdot \sin\varpi_C^* \sin\varpi_D^* - \xi_1 \cdot \cos\varpi_C^* \sin\varpi_D^* - \xi_2 \cdot \cos\varpi_C^* \cos\varpi_D^* = 0 \tag{48}$$

where ϖ_C^*, ϖ_D^* are the mean arguments of latitude corresponding to extreme value points.

Denoting

$$\lambda_x \triangleq \tan\frac{\varpi_C^*}{2}, \quad \eta_x \triangleq \tan\frac{\varpi_D^*}{2} \tag{49}$$

Eqs. (47) and (48) are transformed into a set of quartic equations with two unknown variables λ_x and η_x.

$$(\xi_4 - \xi_6)\lambda_x^2\eta_x^2 + 2(\xi_1 + \xi_5)\lambda_x\eta_x^2 - 2\xi_3\lambda_x^2\eta_x - (\xi_4 + \xi_6)\lambda_x^2 - (\xi_4 - \xi_6)\eta_x^2 + 4\xi_2\lambda_x\eta_x + 2(\xi_5 - \xi_1)\lambda_x + 2\xi_3\eta_x + (\xi_4 + \xi_6) = 0 \tag{50}$$

$$\xi_2\lambda_x^2\eta_x^2 + 2\xi_3\lambda_x\eta_x^2 - 2\xi_1\lambda_x^2\eta_x - \xi_2\lambda_x^2 - \xi_2\eta_x^2 + 4\xi_4\lambda_x\eta_x - 2\xi_3\lambda_x + 2\xi_1\eta_x + \xi_2 = 0 \tag{51}$$

or

$$\lambda_x = \pm\infty \quad \text{or} \quad \eta_x = \pm\infty \tag{52}$$

Note that the mapping in Eq. (49) is discontinuous at the point $\varpi_C^* = \pi$ and $\varpi_D^* = \pi$, which corresponds to the condition of $\lambda_x = \pm\infty$ and $\eta_x = \pm\infty$. Given a favorable initial guess, Eqs. (50) and (51) can be solved in Matlab®. Accordingly, ϖ_C^* and ϖ_D^* can be obtained from Eq. (49). Moreover, we should further check whether $\lambda_x = \pm\infty$ or $\eta_x = \pm\infty$ correspond to the extreme value points by examining Eqs (47) and (48). Note that the number of solutions is infinite because of the existing periodic terms in Eqs. (47) and (48). Substituting ϖ_C^* and ϖ_D^* into Eq. (28) yields the extreme values of *x* components.

For example, assume the displaced orbital elements of the two sails are given by Eq. (39). Solving Eqs. (50), (51) and (52) for λ_x and η_x yields 4 possible solutions:

$$\left(\lambda_{x1}=0,\eta_{x1}=1\right);\quad \left(\lambda_{x2}=0,\eta_{x2}=-1\right);\quad \left(\lambda_{x3}=\pm\infty,\eta_{x3}=1\right);\quad \left(\lambda_{x4}=\pm\infty,\eta_{x4}=-1\right) \tag{53}$$

The mean arguments of latitude corresponding to these solutions are obtained from Eq. (49):

$$\varpi_C^*=k\pi,\quad \varpi_D^*=k\pi+\pi/2 \tag{54}$$

where $k\in\mathbb{Z}$. Substituting ϖ_C^* and ϖ_D^* into Eq. (28) yields four normalized extreme value points:

$$\tilde{x}_1^*=-1.4959956;\quad \tilde{x}_2^*=0.0101092;\quad \tilde{x}_3^*=-0.1040044;\quad \tilde{x}_4^*=-1.6101092 \tag{55}$$

Fig. 7 shows the contour lines of normalized radial distance as a function of mean arguments of latitude of two sails, assuming $\varpi_C,\varpi_D\in[0,2\pi]$, and "$*$" denoting the extreme value points. The solutions given by Eq. (55) can be further verified by Fig. 3.

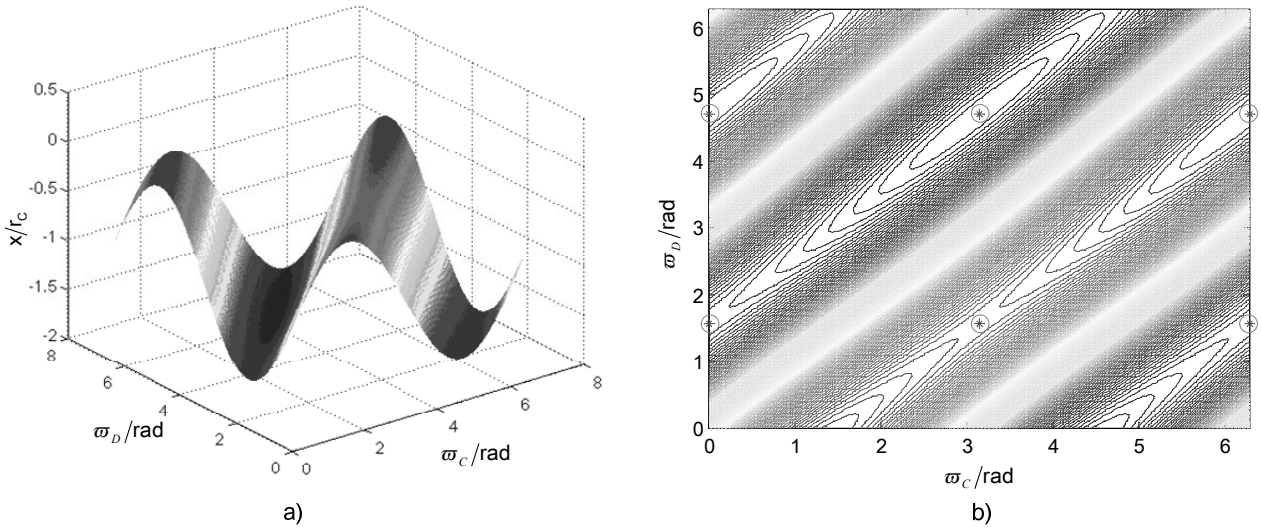

Fig. 7 Normalized radial distance: a) 3-D view. b) Contour plot.

4.1.2 Along-track bounds

Likewise, to gain the bounds of along-track motion, the derivative of y with respect to ϖ_C and ϖ_D must be set equal to zero

$$\frac{\partial y}{\partial \varpi_C}=a_D\sum_{k=1}^{3}\frac{\partial T_C(k,2)}{\partial \varpi_C}T_D(k,1)+H_D\sum_{k=1}^{3}\frac{\partial T_C(k,2)}{\partial \varpi_C}T_D(k,3)=0 \tag{56}$$

$$\frac{\partial y}{\partial \varpi_D}=a_D\sum_{k=1}^{3}T_C(k,2)\frac{\partial T_D(k,1)}{\partial \varpi_D}+H_D\sum_{k=1}^{3}T_C(k,2)\frac{\partial T_D(k,3)}{\partial \varpi_D}=0 \tag{57}$$

which lead to

$$\xi_4\cdot\sin\varpi_C^*\cos\varpi_D^*+\xi_3\cdot\sin\varpi_C^*\sin\varpi_D^*-\xi_2\cdot\cos\varpi_C^*\sin\varpi_D^*+\xi_1\cdot\cos\varpi_C^*\cos\varpi_D^*+\xi_6\cdot\sin\varpi_C^*-\xi_5\cdot\cos\varpi_C^*=0 \tag{58}$$

$$\xi_2\cdot\sin\varpi_C^*\cos\varpi_D^*+\xi_1\cdot\sin\varpi_C^*\sin\varpi_D^*-\xi_4\cdot\cos\varpi_C^*\sin\varpi_D^*+\xi_3\cdot\cos\varpi_C^*\cos\varpi_D^*=0 \tag{59}$$

Denoting

$$\lambda_y\triangleq\tan\frac{\varpi_C^*}{2},\quad \eta_y\triangleq\tan\frac{\varpi_D^*}{2} \tag{60}$$

Eqs. (58) and (59) are therefore transformed into a set of quartic equations with two unknown variables λ_y and η_y.

$$\left(\xi_1+\xi_5\right)\lambda_y^2\eta_y^2+2\left(\xi_6-\xi_4\right)\lambda_y\eta_y^2+2\xi_2\lambda_y^2\eta_y+\left(\xi_5-\xi_1\right)\lambda_y^2-\left(\xi_1+\xi_5\right)\eta_y^2+4\xi_3\lambda_y\eta_y+2\left(\xi_4+\xi_6\right)\lambda_y-2\xi_2\eta_y+\left(\xi_1-\xi_5\right)=0 \quad (61)$$

$$\xi_3\lambda_y^2\eta_y^2-2\xi_2\lambda_y\eta_y^2+2\xi_4\lambda_y^2\eta_y-\xi_3\lambda_y^2-\xi_3\eta_y^2+4\xi_1\lambda_y\eta_y+2\xi_2\lambda_y-2\xi_4\eta_y+\xi_3=0 \quad (62)$$

or

$$\lambda_y=\pm\infty \quad \text{or} \quad \eta_y=\pm\infty \quad (63)$$

The set of quartic equations Eqs. (61) and (62) can be solved to get λ_y and η_y, hence ϖ_C^*, ϖ_D^* are obtained from Eq.(60). However, we should further check whether $\lambda_y=\pm\infty$ or $\eta_y=\pm\infty$ correspond to the extreme value points by examining Eqs. (58) and (59). Substituting ϖ_C^* and ϖ_D^* into Eq. (28) yields the extreme values of *y* components.

Utilizing the same displaced orbital elements by Eq. (39) and solving Eqs. (61), (62) and (63) yields four possible solutions:

$$\left(\lambda_{y1}=1,\eta_{y1}=1\right);\quad \left(\lambda_{y2}=1,\eta_{y2}=-1\right);\quad \left(\lambda_{y3}=-1,\eta_{y3}=1\right);\quad \left(\lambda_{y4}=-1,\eta_{y4}=-1\right) \quad (64)$$

Eq. (60) provides the corresponding mean arguments of latitude regarding to these solutions:

$$\varpi_C^*=k\pi+\pi/2,\quad \varpi_D^*=k\pi+\pi/2 \quad (65)$$

Substituting ϖ_C^* and ϖ_D^* into Eq. (28) yields four normalized extreme value points:

$$\tilde{y}_1^*=0.6959956;\quad \tilde{y}_2^*=-0.8101092;\quad \tilde{y}_3^*=-0.6959956;\quad \tilde{y}_4^*=0.8101092 \quad (66)$$

Fig. 8 shows the contour lines of normalized along-track distance as a function of mean arguments of latitude of two sails. It can be clear seen that the extreme value points given by Eq. (66) are exactly the along-track bounds exhibited in Fig. 3.

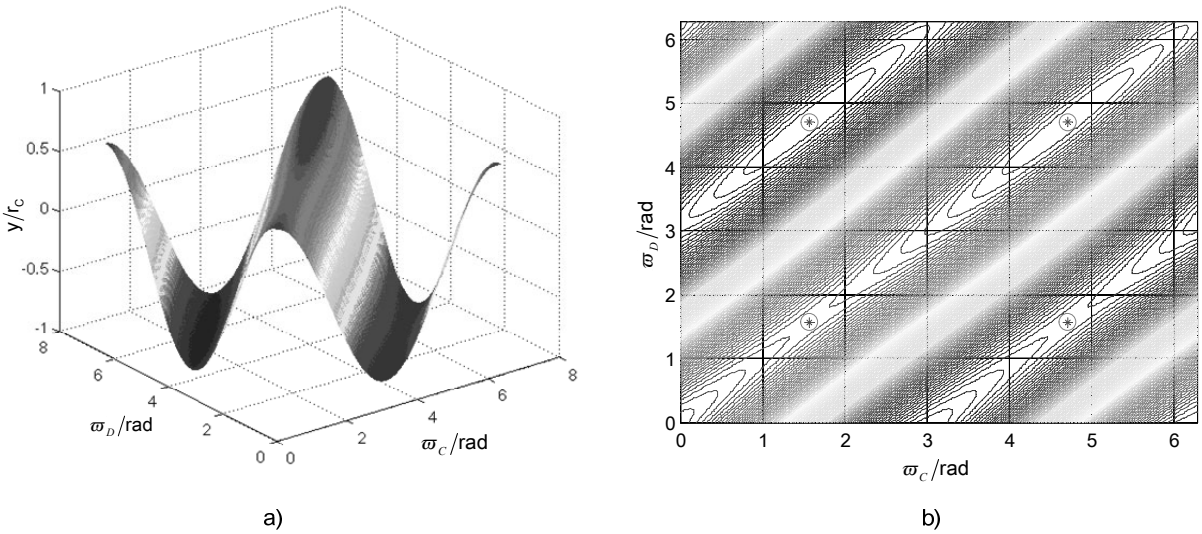

a) b)

Fig. 8 Normalized along-track distance: a) 3-D view. b) Contour plot.

4.1.3 Cross-track bounds

To acquire the bounds of cross-track motion, the following relationship should hold

$$\frac{\partial z}{\partial \varpi_C}=a_D\sum_{k=1}^{3}\frac{\partial T_C(k,3)}{\partial \varpi_C}T_D(k,1)+H_D\sum_{k=1}^{3}\frac{\partial T_C(k,3)}{\partial \varpi_C}T_D(k,3)=0 \quad (67)$$

$$\frac{\partial z}{\partial \varpi_D}=a_D\sum_{k=1}^{3}T_C(k,3)\frac{\partial T_D(k,1)}{\partial \varpi_D}+H_D\sum_{k=1}^{3}T_C(k,3)\frac{\partial T_D(k,3)}{\partial \varpi_D}=0 \quad (68)$$

Note that

$$\frac{\partial T_C(k,3)}{\partial \varpi_C} = 0, \quad k = 1,2,3 \tag{69}$$

Hence Eqs. (67) and (68) become

$$\xi_7 \cdot \sin \varpi_D^* + \xi_8 \cos \varpi_D^* = 0 \tag{70}$$

Denoting

$$\eta_z \triangleq \tan \frac{\varpi_D^*}{2} \tag{71}$$

Eq. (71) is therefore transformed into a quadratic equation with only one unknown variables η_z.

$$\xi_8 \eta_z^2 - 2\xi_7 \eta_z - \xi_8 = 0 \tag{72}$$

or

$$\eta_z = \pm\infty \tag{73}$$

Eq. (72) is solved as

$$\eta_z = \frac{\xi_7 \pm \sqrt{\xi_7^2 + \xi_8^2}}{\xi_8} \tag{74}$$

Then we obtain ϖ_D^* from Eq. (71). Substituting ϖ_D^* into Eq. (28) yields the extreme values of *z* components.

With the previously given displaced orbital elements, we have

$$\eta_{z1} = 1; \quad \eta_{z2} = -1; \tag{75}$$

Substituting Eq. (75) into Eq. (71) yields

$$\varpi_D^* = k\pi + \pi/2 \tag{76}$$

And the two normalized extreme value points are obtained by substituting ϖ_D^* into Eq. (28):

$$\tilde{z}_1^* = 0.1180461; \quad \tilde{z}_2^* = -0.0137210 \tag{77}$$

Fig. 9 illustrates the variation of normalized cross-track distance as a function of deputy sail's mean argument of latitude. The extreme value points given by Eq. (77) are in accordance with the numerical representation, verifying the correctness of the proposed method.

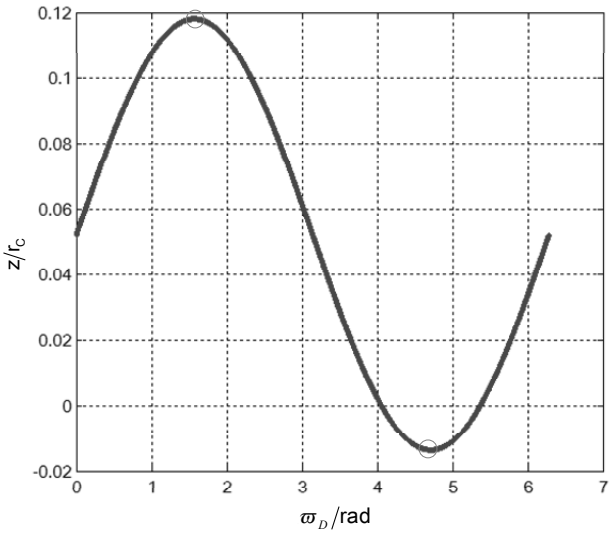

Fig. 9 Normalized cross-track distance

4.1.4 Relative distance bounds

Let $\rho = \|\boldsymbol{\rho}\|$, to seek for the extreme values of relative distance, the necessary conditions are

$$\frac{\partial \rho^2}{\partial \varpi_C} = 2x \cdot \frac{\partial x}{\partial \varpi_C} + 2y \cdot \frac{\partial y}{\partial \varpi_C} + 2z \cdot \frac{\partial z}{\partial \varpi_C} = 0 \tag{78}$$

$$\frac{\partial \rho^2}{\partial \varpi_D} = 2x \cdot \frac{\partial x}{\partial \varpi_D} + 2y \cdot \frac{\partial y}{\partial \varpi_D} + 2z \cdot \frac{\partial z}{\partial \varpi_D} = 0 \tag{79}$$

Unlike the method that calculates the extreme value points of radial, along-track and cross-track motion, Eqs. (78) and (79) will result in an equation of degree 8, and in the general cases, the expression of relative distance is difficult to be further simplified into a concise form. However, under some conditions, for example, when $i_C, i_D = 0^\circ, 90^\circ$ or $\Omega_C = \Omega_D$, the problem degenerates, and the search for extreme values of relative distance bounds can be transformed into seeking for the solution of two simple equations. Utilizing the displaced orbital elements of the two sails given by Eq. (39), Eqs. (78) and (79) result in

$$-\iota_1 \sin\varpi_C \sin\varpi_D + \iota_2 \cos\varpi_C \cos\varpi_D - \iota_3 \sin\varpi_C = 0 \tag{80}$$

$$\iota_1 \cos\varpi_C \cos\varpi_D - \iota_2 \sin\varpi_C \sin\varpi_D + \iota_4 \cos\varpi_D = 0 \tag{81}$$

where

$$\iota_1 \triangleq 2a_C a_D \cos i_D, \quad \iota_2 \triangleq -2a_C a_D, \quad \iota_3 \triangleq -2a_C H_D \sin i_D, \quad \iota_4 \triangleq -2H_C a_D \sin i_D \tag{82}$$

Eqs. (80) and (81) can be solved easily, and the mean arguments of latitude of extreme value points are

$$\varpi_C^* = k\pi, \quad \varpi_D^* = k\pi + \pi/2 \tag{83}$$

The relative distance bounds are

$$\rho_1^* = \sqrt{\iota_0 + \iota_1 + \iota_3 + \iota_4}, \quad \rho_2^* = \sqrt{\iota_0 - \iota_1 + \iota_3 - \iota_4}, \quad \rho_1^* = \sqrt{\iota_0 - \iota_1 - \iota_3 + \iota_4}, \quad \rho_1^* = \sqrt{\iota_0 + \iota_1 - \iota_3 - \iota_4} \tag{84}$$

where

$$\iota_0 \triangleq a_C^2 + a_D^2 + H_C^2 + H_D^2 - 2H_C H_D \cos i_D \tag{85}$$

The normalized extreme value points are calculated from Eq. (84) as

$$\tilde{\rho}_1^* = 1.5006457; \quad \tilde{\rho}_2^* = 0.0170430; \quad \tilde{\rho}_3^* = 0.1573270; \quad \tilde{\rho}_4^* = 1.6101677 \tag{86}$$

Fig. 10 illustrates the contour lines of normalized relative distance as a function of mean arguments of latitude of two sails, verifying the correctness of the presented method.

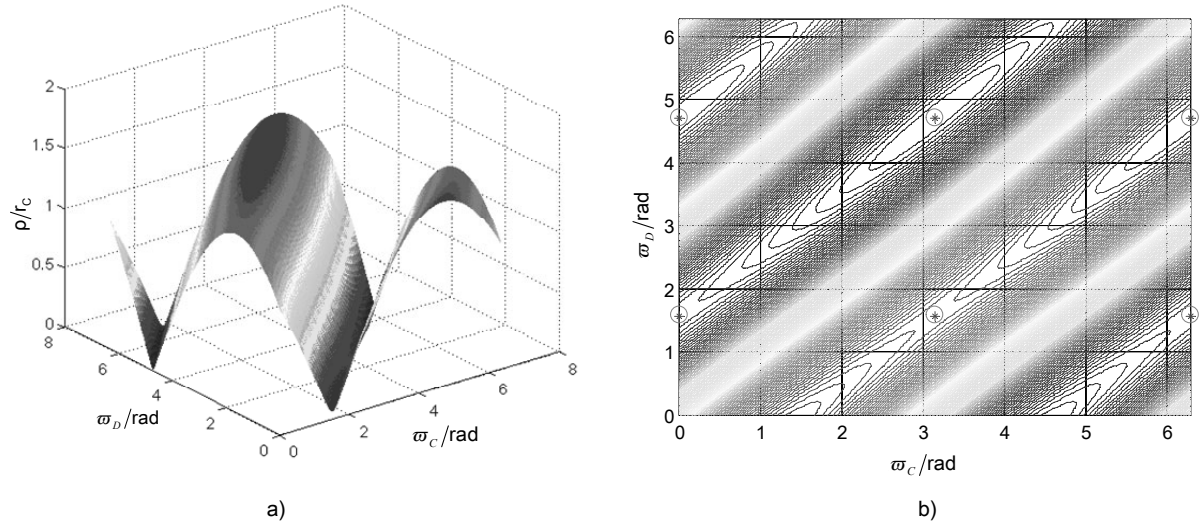

a) b)

Fig. 10 Normalized relative distance: a) 3-D view. b) Contour plot.

4.2 Bounds of 1:1 Commensurability Relative Orbit

To find the bounds of incommensurable relative orbit, the mean arguments of latitude of the two sails are treated as variables that are independent of each other, due to their ergodic nature. However for the commensurable case, time is the only variable. To determine the bounds of directional components, the following relationship should hold:

$$\frac{\partial \boldsymbol{\rho}}{\partial \boldsymbol{t}} = \frac{\partial \boldsymbol{\rho}}{\partial \boldsymbol{\varpi}_C} \cdot \frac{\partial \boldsymbol{\varpi}_C}{\partial \boldsymbol{t}} + \frac{\partial \boldsymbol{\rho}}{\partial \boldsymbol{\varpi}_D} \cdot \frac{\partial \boldsymbol{\varpi}_D}{\partial \boldsymbol{t}} = \boldsymbol{0}_{3\times 1} \tag{87}$$

where $\boldsymbol{t} = \left[t_x, t_y, t_z \right]^T$. Consider the 1:1 commensurable case, so that

$$\omega_C = \omega_D = \omega \tag{88}$$

Therefore, Eq. (87) results in

$$\frac{\partial x}{\partial \varpi_C} + \frac{\partial x}{\partial \varpi_D} = \frac{\partial y}{\partial \varpi_C} + \frac{\partial y}{\partial \varpi_D} = \frac{\partial z}{\partial \varpi_C} + \frac{\partial z}{\partial \varpi_D} = 0 \tag{89}$$

Denote

$$\gamma_C \triangleq \tan\frac{\varpi_{C0}}{2}, \quad \gamma_D \triangleq \tan\frac{\varpi_{D0}}{2} \tag{90}$$

where ϖ_{C_0} and ϖ_{D_0} are defined in Eq. (41), and

$$\chi_x \triangleq \tan\frac{\omega t_x^*}{2}, \quad \chi_y \triangleq \tan\frac{\omega t_y^*}{2}, \quad \chi_z \triangleq \tan\frac{\omega t_z^*}{2} \tag{91}$$

where t_x^*, t_y^* and t_z^* represent the times corresponding to extreme value points of directional components. Substituting Eqs. (41), (42), (90) and (91) into Eq. (89) leads to

$$\sigma_4 \chi_x^4 + \sigma_3 \chi_x^3 + \sigma_2 \chi_x^2 + \sigma_1 \chi_x + \sigma_0 = 0 \tag{92}$$

$$\tau_4 \chi_y^4 + \tau_3 \chi_y^3 + \tau \chi_y^2 + \tau_1 \chi_y + \tau_0 = 0 \tag{93}$$

$$\zeta_2 \chi_z^2 + \zeta_1 \chi_z + \zeta_0 = 0 \tag{94}$$

Because the expressions of the coefficients σ_i, τ_i and ζ_i are too complex, they are given in Appendix.

Solving Eqs. (92), (93) and (94) yields the times corresponding to extreme points. Hence the bounds of radial, along-track and cross-track motion can be calculated respectively according to Eqs. (41) and (42).

Likewise, to calculate the relative distance bounds, the following expression should be satisfied

$$\frac{\partial \rho^2}{\partial t} = \frac{\partial \rho^2}{\partial \varpi_C} \cdot \frac{\partial \varpi_C}{\partial t} + \frac{\partial \rho^2}{\partial \varpi_D} \cdot \frac{\partial \varpi_D}{\partial t} = 0 \tag{95}$$

Recalling Eq. (88), we have

$$\frac{\partial \rho^2}{\partial \varpi_C} + \frac{\partial \rho^2}{\partial \varpi_D} = 0 \tag{96}$$

Utilizing the displaced orbital elements of the two sails given by Eq. (39) and substituting them into Eq. (92), we obtain

$$\chi_x = \frac{\kappa_3 + \sqrt{\kappa_3^2 + 8\left(\kappa_2 - \kappa_1\right)^2}}{2\left(\kappa_2 - \kappa_1\right)} \pm \sqrt{1 + \frac{\kappa_3^2 + \kappa_3\sqrt{\kappa_3^2 + 8\left(\kappa_2 - \kappa_1\right)^2}}{2\left(\kappa_2 - \kappa_1\right)^2}} \tag{97}$$

After some mathematical operations, the normalized times corresponding to extreme value points of radial motion are calculated from Eq. (91) as

$$\tilde{t}^*_{x\_\max} = \frac{1}{\tilde{\omega}}\left\{2k\pi + \arcsin\left[\frac{-\kappa_3 + \sqrt{\kappa_3^2 + 8\left(\kappa_2 - \kappa_1\right)^2}}{4\left(\kappa_2 - \kappa_1\right)}\right]\right\} \tag{98}$$

$$\tilde{t}^*_{x\_\min} = \frac{1}{\tilde{\omega}}\left\{(2k+1)\pi - \arcsin\left[\frac{-\kappa_3 + \sqrt{\kappa_3^2 + 8\left(\kappa_2 - \kappa_1\right)^2}}{4\left(\kappa_2 - \kappa_1\right)}\right]\right\} \tag{99}$$

Substituting Eqs. (98) and (99) into Eq. (42) yields the normalized bounds of radial motion $\tilde{x}_{\max}$ and $\tilde{x}_{\min}$。

Fig. 11 shows the variation of radial distance within one period, namely $\tilde{t} \in [0, 4\pi]$. Eqs. (98) and (99) result in $\tilde{t}^*_{x\_\max} = 0.1003653$, $\tilde{t}^*_{x\_\min} = 6.1828200$, and the radial bounds are $\tilde{x}_{\max} = -0.7428709$, $\tilde{x}_{\min} = -0.8571291$.

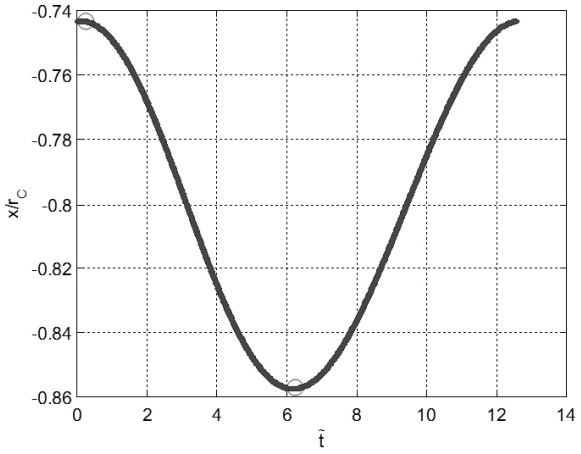

Fig. 11 The variation of radial distance.

Likewise, Eq. (93) leads to

$$\chi_y = \pm 1 \tag{100}$$

The normalized times corresponding to extreme value points of along-track motion are calculated from Eq. (91) as

$$\tilde{t}^*_{y\_\max} = \frac{1}{\tilde{\omega}}\left(2k + \frac{3}{2}\right)\pi \tag{101}$$

$$\tilde{t}^*_{y\_\min} = \frac{1}{\tilde{\omega}}\left(2k + \frac{1}{2}\right)\pi \tag{102}$$

The normalized bounds of along-track motion $\tilde{y}_{\max}$ and $\tilde{y}_{\min}$ are obtained by substituting Eqs. (101) and (102) into Eq. (42).

Fig. 12 illustrates the variation of along-track distance within one period. From Eqs. (101) and (102), we obtain $\tilde{t}^*_{y\_\max} = 9.4247780$, $\tilde{t}^*_{y\_\min} = 3.1415927$, and the along-track bounds are $\tilde{y}_{\max} = 0.8101092$, $\tilde{y}_{\min} = 0.6959956$.

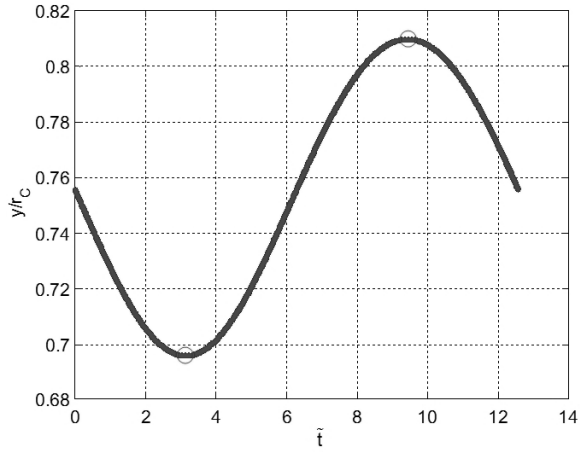

Fig. 12 The variation of along-track distance.

Likewise, Eq. (94) results in

$$\chi_z = \pm 1 \tag{103}$$

The normalized times corresponding to extreme value points of cross-track motion are calculated from Eq. (91) as

$$\tilde{t}^*_{z\_\max} = \frac{1}{\tilde{\omega}}\left(2k + \frac{1}{2}\right)\pi \tag{104}$$

$$\tilde{t}^*_{z\_\min} = \frac{1}{\tilde{\omega}}\left(2k + \frac{3}{2}\right)\pi \tag{105}$$

Substituting Eqs. (104) and (105) into Eq. (42) yields the normalized bounds of cross-track motion $\tilde{z}_{\max}$ and $\tilde{z}_{\min}$.

Fig. 13 shows the variation of cross-track distance within one period. From Eqs. (104) and (105), we obtain $\tilde{t}^*_{z\_\max} = 3.1415927$, $\tilde{t}^*_{z\_\min} = 9.4247780$, and the cross-track bounds are $\tilde{z}_{\max} = 0.1180461$, $\tilde{z}_{\min} = -0.0137210$.

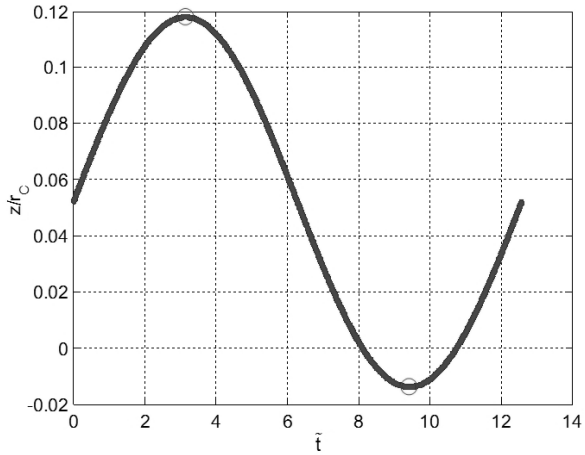

Fig. 13 The variation of cross-track distance.

In order to find the bounds of relative distance between two displaced orbits, substitute Eq. (96) into Eq. (42) to obtain

$$-2\kappa_3\kappa_4\varsigma + 2\left(\kappa_5\kappa_6 - \kappa_1\kappa_3\right)\sqrt{1-\varsigma^2} + 2\left(\kappa_1^2 + \kappa_5^2 - \kappa_2^2\right)\varsigma\sqrt{1-\varsigma^2} + 2\left(\kappa_4\kappa_2 - \kappa_4\kappa_1\right)\left(1-2\varsigma^2\right) = 0 \tag{106}$$

where

$$\varsigma \triangleq \sin\left(\tilde{\omega}\tilde{t}^*_\rho\right) \tag{107}$$

Theoretically, Eq. (106) has four roots, but only two are meaningful:

$$\varsigma_1 = 0.6584719, \quad \varsigma_2 = -0.6501913$$

The normalized times corresponding to extreme value points of relative distance are calculated as

$$\tilde{t}^*_{\rho\_\max} = \frac{1}{\tilde{\omega}}\left(2k\pi + \arcsin\varsigma_1\right) \tag{108}$$

$$\tilde{t}^*_{\rho\_\min} = \frac{1}{\tilde{\omega}}\left[\left(2k+1\right)\pi + \arcsin\varsigma_2\right] \tag{109}$$

Fig. 14 shows the variation of relative distance within one period. From Eqs. (108) and (109), we obtain $\tilde{t}^*_{\rho\_\max} = 1.4375732$, $\tilde{t}^*_{\rho\_\min} = 7.6988577$, and the relative distance bounds are $\tilde{\rho}_{\max} = 1.1558096$, $\tilde{\rho}_{\min} = 1.0461162$.

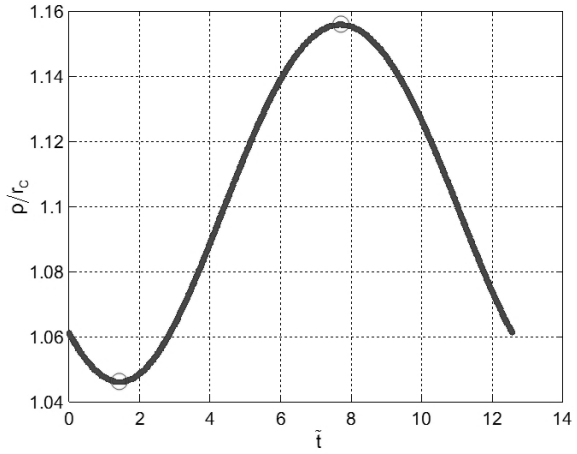

Fig. 14 The variation of relative distance.

5. Conclusions

A new set of displaced orbital elements has been introduced to describe the position of displaced orbits, by means of which, the relative motion between heliocentric displaced orbits can be modeled in the chief sail's rotating frame, and a closed form solution to the relative motion problem between displaced orbits were obtained. Utilizing the displaced orbital elements, the invariant manifold of relative motion can be determined. The orbits evolving on the manifold manifest periodicity for the commensurable case and quasi-periodicity (ergodicity) for the incommensurable case.

The bounds of relative motion between displaced orbits have been calculated from an analytic point of view both for the incommensurable and 1:1 commensurable case. A few important conclusions can be drawn from these calculations. It was found that for the incommensurable case, there are four extreme values for the radial, along-track motion and relative distance, and two for the cross-track motion. For the 1:1 commensurable case, these values reduce to two. Some illustrative examples have been carried out to verify the effectiveness of the proposed theory.

The derived expressions of quantitative relative distance bounds are of fundamental importance, because the knowledge of maximum distance is crucial for communication design whereas minimum distance is essential for collision avoidance.

Acknowledgements

This work was supported by the National Natural Science Foundation of China (No. 11472213) and Open Research Foundation of Science and Technology in Aerospace Flight Dynamics Laboratory of China (No. 2015afdl016). This work was also funded by Chinese Scholarship Council.

Appendix: Relevant Coefficients in Eqs. (92), (93) and (94)

The coefficients $\sigma_0 \sim \sigma_4$, $\tau_0 \sim \tau_4$, $\zeta_0 \sim \zeta_2$ in Eqs. (92), (93) and (94) are given by

$$\begin{aligned}\sigma_4 &= (\xi_4 - \xi_6 - \xi_2) - 2(\xi_1 + \xi_5 - \xi_3)\gamma_C - 2(\xi_1 - \xi_3)\gamma_D + (\xi_2 - \xi_4 - \xi_6)\gamma_D^2 + (\xi_2 + \xi_6 - \xi_4)\gamma_C^2 + 4(\xi_2 - \xi_4)\gamma_C\gamma_D \\ &\quad -2(\xi_3 + \xi_5 - \xi_1)\gamma_C\gamma_D^2 - 2(\xi_3 - \xi_1)\gamma_C^2\gamma_D + (\xi_4 + \xi_6 - \xi_2)\gamma_C^2\gamma_D^2\end{aligned}$$

$$\begin{aligned}\sigma_3 &= 2(\xi_4 - \xi_6 - \xi_2)(\gamma_C + \gamma_D) + 2(\xi_1 + \xi_5 - \xi_3)(1 - \gamma_C^2 - 2\gamma_C\gamma_D) + 2(\xi_1 - \xi_3)(1 - \gamma_D^2 - 2\gamma_C\gamma_D) \\ &\quad +2(\xi_2 - \xi_4 - \xi_6)(\gamma_C\gamma_D^2 - \gamma_D) + 2(\xi_2 + \xi_6 - \xi_4)(\gamma_C^2\gamma_D - \gamma_C) + 4(\xi_2 - \xi_4)(\gamma_C^2\gamma_D + \gamma_C\gamma_D^2 - \gamma_C - \gamma_D) \\ &\quad +2(\xi_3 + \xi_5 - \xi_1)(2\gamma_C\gamma_D + \gamma_D^2 - \gamma_C^2\gamma_D^2) + 2(\xi_3 - \xi_1)(2\gamma_C\gamma_D + \gamma_C^2 - \gamma_C^2\gamma_D^2) - 2(\xi_4 + \xi_6 - \xi_2)(\gamma_C^2\gamma_D + \gamma_C\gamma_D^2)\end{aligned}$$

$$\begin{aligned}\sigma_2 &= (\xi_4 - \xi_6 - \xi_2)(\gamma_C^2 + \gamma_D^2 + 4\gamma_C\gamma_D) + 2(\xi_1 + \xi_5 - \xi_3)(\gamma_C + 2\gamma_D - 2\gamma_C^2\gamma_D - \gamma_C\gamma_D^2) + 2(\xi_1 - \xi_3)(\gamma_D + 2\gamma_C - 2\gamma_C\gamma_D^2 - \gamma_C^2\gamma_D) \\ &\quad +(\xi_2 - \xi_4 - \xi_6)(1 - 4\gamma_C\gamma_D + \gamma_C^2\gamma_D^2) + (\xi_2 + \xi_6 - \xi_4)(1 - 4\gamma_C\gamma_D + \gamma_C^2\gamma_D^2) + 4(\xi_2 - \xi_4)(1 - \gamma_C^2 - 2\gamma_C\gamma_D - \gamma_D^2 + \gamma_C^2\gamma_D^2) \\ &\quad +2(\xi_3 + \xi_5 - \xi_1)(2\gamma_C^2\gamma_D + \gamma_C\gamma_D^2 - \gamma_C - 2\gamma_D) + 2(\xi_3 - \xi_1)(2\gamma_C\gamma_D^2 + \gamma_C^2\gamma_D - \gamma_D - 2\gamma_C) + (\xi_4 + \xi_6 - \xi_2)(\gamma_C^2 + \gamma_D^2 + 4\gamma_C\gamma_D)\end{aligned}$$

$$\begin{aligned}\sigma_1 &= 2(\xi_4 - \xi_6 - \xi_2)(\gamma_C^2\gamma_D + \gamma_C\gamma_D^2) + 2(\xi_1 + \xi_5 - \xi_3)(\gamma_D^2 + 2\gamma_C\gamma_D - \gamma_C^2\gamma_D^2) + 2(\xi_1 - \xi_3)(\gamma_C^2 + 2\gamma_C\gamma_D - \gamma_C^2\gamma_D^2) \\ &\quad +2(\xi_2 - \xi_4 - \xi_6)(\gamma_C - \gamma_C^2\gamma_D) + 2(\xi_2 + \xi_6 - \xi_4)(\gamma_D - \gamma_C\gamma_D^2) + 4(\xi_2 - \xi_4)(\gamma_C + \gamma_D - \gamma_C^2\gamma_D - \gamma_C\gamma_D^2) \\ &\quad +2(\xi_3 + \xi_5 - \xi_1)(1 - 2\gamma_C\gamma_D - \gamma_C^2) + 2(\xi_3 - \xi_1)(1 - 2\gamma_C\gamma_D - \gamma_D^2) - 2(\xi_4 + \xi_6 - \xi_2)(\gamma_C + \gamma_D)\end{aligned}$$

$$\begin{aligned}\sigma_0 &= 2(\xi_4 - \xi_6 - \xi_2)\gamma_C^2\gamma_D^2 + 2(\xi_1 + \xi_5 - \xi_3)\gamma_C\gamma_D^2 + 2(\xi_1 - \xi_3)\gamma_C^2\gamma_D + 2(\xi_2 - \xi_4 - \xi_6)\gamma_C^2 + 2(\xi_2 + \xi_6 - \xi_4)\gamma_D^2 \\ &\quad +4(\xi_2 - \xi_4)\gamma_C\gamma_D + 2(\xi_3 + \xi_5 - \xi_1)\gamma_C + 2(\xi_3 - \xi_1)\gamma_D + (\xi_4 + \xi_6 - \xi_2)\end{aligned}$$

$$\begin{aligned}\tau_4 &= (\xi_1 + \xi_5 - \xi_3) - 2(\xi_2 + \xi_6 - \xi_4)\gamma_C - 2(\xi_2 - \xi_4)\gamma_D + (\xi_3 + \xi_5 - \xi_1)\gamma_D^2 + (\xi_3 - \xi_1 - \xi_5)\gamma_C^2 + 4(\xi_3 - \xi_1)\gamma_C\gamma_D \\ &\quad -2(\xi_4 + \xi_6 - \xi_2)\gamma_C\gamma_D^2 - 2(\xi_4 - \xi_2)\gamma_C^2\gamma_D + (\xi_1 - \xi_3 - \xi_5)\gamma_C^2\gamma_D^2\end{aligned}$$

$$\begin{aligned}\tau_3 &= 2(\xi_1 + \xi_5 - \xi_3)(\gamma_C + \gamma_D) + 2(\xi_2 + \xi_6 - \xi_4)(1 - \gamma_C^2 - 2\gamma_C\gamma_D) + 2(\xi_2 - \xi_4)(1 - \gamma_D^2 - 2\gamma_C\gamma_D) \\ &\quad +2(\xi_3 + \xi_5 - \xi_1)(\gamma_C\gamma_D^2 - \gamma_D) + 2(\xi_3 - \xi_1 - \xi_5)(\gamma_C^2\gamma_D - \gamma_C) + 4(\xi_3 - \xi_1)(\gamma_C^2\gamma_D + \gamma_C\gamma_D^2 - \gamma_C - \gamma_D) \\ &\quad +2(\xi_4 + \xi_6 - \xi_2)(2\gamma_C\gamma_D + \gamma_D^2 - \gamma_C^2\gamma_D^2) + 2(\xi_4 - \xi_2)(2\gamma_C\gamma_D + \gamma_C^2 - \gamma_C^2\gamma_D^2) - 2(\xi_1 - \xi_3 - \xi_5)(\gamma_C^2\gamma_D + \gamma_C\gamma_D^2)\end{aligned}$$

$$\begin{aligned}\tau_2 &= (\xi_1 + \xi_5 - \xi_3)(\gamma_C^2 + \gamma_D^2 + 4\gamma_C\gamma_D) + 2(\xi_2 + \xi_6 - \xi_4)(\gamma_C + 2\gamma_D - 2\gamma_C^2\gamma_D - \gamma_C\gamma_D^2) + 2(\xi_2 - \xi_4)(\gamma_D + 2\gamma_C - 2\gamma_C\gamma_D^2 - \gamma_C^2\gamma_D) \\ &\quad +(\xi_3 + \xi_5 - \xi_1)(1 - 4\gamma_C\gamma_D + \gamma_C^2\gamma_D^2) + (\xi_3 - \xi_1 - \xi_5)(1 - 4\gamma_C\gamma_D + \gamma_C^2\gamma_D^2) + 4(\xi_3 - \xi_1)(1 - \gamma_C^2 - 2\gamma_C\gamma_D - \gamma_D^2 + \gamma_C^2\gamma_D^2) \\ &\quad +2(\xi_4 + \xi_6 - \xi_2)(2\gamma_C^2\gamma_D + \gamma_C\gamma_D^2 - \gamma_C - 2\gamma_D) + 2(\xi_4 - \xi_2)(2\gamma_C\gamma_D^2 + \gamma_C^2\gamma_D - \gamma_D - 2\gamma_C) + (\xi_1 - \xi_3 - \xi_5)(\gamma_C^2 + \gamma_D^2 + 4\gamma_C\gamma_D)\end{aligned}$$

$$\begin{aligned}\tau_1 &= 2(\xi_1 + \xi_5 - \xi_3)(\gamma_C^2\gamma_D + \gamma_C\gamma_D^2) + 2(\xi_2 + \xi_6 - \xi_4)(\gamma_D^2 + 2\gamma_C\gamma_D - \gamma_C^2\gamma_D^2) + 2(\xi_2 - \xi_4)(\gamma_C^2 + 2\gamma_C\gamma_D - \gamma_C^2\gamma_D^2) \\ &\quad +2(\xi_3 + \xi_5 - \xi_1)(\gamma_C - \gamma_C^2\gamma_D) + 2(\xi_3 - \xi_1 - \xi_5)(\gamma_D - \gamma_C\gamma_D^2) + 4(\xi_3 - \xi_1)(\gamma_C + \gamma_D - \gamma_C^2\gamma_D - \gamma_C\gamma_D^2) \\ &\quad +2(\xi_4 + \xi_6 - \xi_2)(1 - 2\gamma_C\gamma_D - \gamma_C^2) + 2(\xi_4 - \xi_2)(1 - 2\gamma_C\gamma_D - \gamma_D^2) - 2(\xi_1 - \xi_3 - \xi_5)(\gamma_C + \gamma_D)\end{aligned}$$

$$\begin{aligned}\tau_0 &= 2(\xi_1 + \xi_5 - \xi_3)\gamma_C^2\gamma_D^2 + 2(\xi_2 + \xi_6 - \xi_4)\gamma_C\gamma_D^2 + 2(\xi_2 - \xi_4)\gamma_C^2\gamma_D + 2(\xi_3 + \xi_5 - \xi_1)\gamma_C^2 + 2(\xi_3 - \xi_1 - \xi_5)\gamma_D^2 \\ &\quad +4(\xi_3 - \xi_1)\gamma_C\gamma_D + 2(\xi_4 + \xi_6 - \xi_2)\gamma_C + 2(\xi_4 - \xi_2)\gamma_D + (\xi_1 - \xi_3 - \xi_5)\end{aligned}$$

$$\zeta_2 = \xi_8 + 2\xi_7\gamma_D - \xi_8\gamma_D^2$$

$$\zeta_1 = 4\xi_8\gamma_D + 2\xi_7\gamma_D^2 - 2\xi_7$$

$$\zeta_0 = \xi_8\gamma_D^2 - 2\xi_7\gamma_D - \xi_8$$

References

[1] McInnes, C. R., Solar Sailing: Technology, Dynamics and Mission Applications, Praxis, Chichester, England, U.K., 1999, Chap. 5.

[2] McKay, R. J., Macdonald, M., Biggs, J., and McInnes, C. R., "Survey of Highly-Non-Keplerian Orbits with Low-Thrust Propulsion," Journal of Guidance, Control, and Dynamics, Vol. 34, No. 3, 2011, pp. 645–666.
doi: 10.2514/1.52133

[3] Mengali, G., and Quarta, A. A., "Non-Keplerian Orbits for Electric Sails," Celestial Mechanics and Dynamical Astronomy, Vol. 105, Nos. 1–3, 2009, pp. 179–195.
doi: 10.1007/s10569-009-9200-y

[4] McInnes, C. R., "Solar Sail Mission Applications for Non-Keplerian Orbits," Acta Astronautic, Vol. 45, Nos. 4–9, 1999, pp. 567–575.
doi: 10.1016/S0094-5765(99)00177-0

[5] Macdonald, M., McKay, R. J., Vasile, M., de Frescheville, F. B., Biggs, J., and McInnes, C. R., "Low-Thrust-Enabled Highly-Non-Keplerian Orbits in Support of Future Mars Exploration," Journal of Guidance, Control, and Dynamics, Vol. 34, No. 5, 2011, pp. 1396–1410.
doi: 10.2514/1.52602

[6] Ceriotti, M., Heiligers, J., and McInnes, C. R., "Trajectory and Spacecraft Design for a Pole-Sitter Mission," Journal of Spacecraft and Rockets, Vol. 51, No. 1, 2014, pp. 311–326.
doi: 10.2514/1.A32477

[7] Gong, S. P., Baoyin, H. X., and Li, J. F., "Solar Sail Formation Flying Around Displaced Solar Orbits," Journal of Guidance, Control, and Dynamics, Vol. 30, No. 4, 2007, pp. 1147–1151.
doi: 10.2514/1.24315

[8] Gong, S. P., Baoyin, H. X., and Li, J., "Relative Orbit Design and Control of Formation Around Displaced Solar Orbits," Aerospace Science and Technology, Vol. 12, No. 2, 2008, pp. 195–201.
doi: 10.1016/j.ast.2007.05.004

[9] Gong, S. P., Li, J. F., and Baoyin, H. X., "Formation Around Planetary Displaced Orbits," Applied Mathematics and Mechanics, Vol. 28, No. 6, 2007, pp. 759–767.
doi: 10.1007/s10483-007-0606-y

[10] McInnes, C. R., "The Existence and Stability of Families of Displaced Two-Body Orbits," Celestial Mechanics and Dynamical Astronomy, Vol. 67, No. 2, 1997, pp. 167–180.
doi: 10.1023/A:1008280609889

[11] Broucke, R. A., and Cefola, P. J., "On the Equinoctial Orbit Elements," Celestial Mechanics, Vol. 5, No. 3, 1972, pp. 303–310.
doi: 10.1007/BF01228432

[12] Gurfil, P., "Euler Parameters as Nonsingular Orbital Elements in Near-Equatorial Orbits," Journal of Guidance, Control, and Dynamics, Vol. 28, No. 5, 2005, pp. 1079–1083.
doi: 10.2514/1.14760

[13] Cohen, C. J., and Hubbard, E. C., "A Nonsingular Set of Orbital Elements," Astronomical Journal, Vol. 67, No. 1, 1962, pp. 10–15.
doi: 10.1086/108597

[14] McInnes, C. R., "Passive Control of Displaced Solar Sail Orbits," Journal of Guidance, Control, and Dynamics, Vol. 21, No. 6, 1998, pp. 975–982.
doi: 10.2514/2.4334

[15] Gurfil, P., and Kholshevnikov, K. V., “Manifolds and Metrics in the Relative Spacecraft Motion Problem,” Journal of Guidance, Control, and Dynamics, Vol. 29, No. 4, 2006, pp. 1004–1010.
doi: 10.2514/1.15531

[16] Nayfeh, A. H., and Balachandran B., Applied Nonlinear Dynamics, WILEY-VCH Verlag GmbH & Co. KGaA, Weinheim, 2004, pp. 235–236.

[17] Strogatz, S. H., Nonlinear Dynamics and Chaos, Perseus Books Publishing, L. L. C., 1994, pp. 273–276.